Microstructure and mechanical properties of GTAW welded joints of AA6105 aluminum alloy

Microestructura y propiedades mecánicas de la soldadura GTAW de aluminio AA6105

Microestrutura e propriedades mecânicas da soldadura GTAW de alumínio AA6105

Fecha de recepción: 8 de octubre de 2015
Fecha de aprobación: 2 de junio de 2016

Minerva Dorta-Almenara*
María Cristina Capace**

Abstract

Gas Tungsten Arc Welding (GTAW) is one of the most used methods to weld aluminum. This work investigates the influence of welding parameters on the microstructure and mechanical properties of GTAW welded AA6105 aluminum alloy joints. AA6105 alloy plates with different percent values of cold work were joined by GTAW, using various combinations of welding current and speed. The fusion zone, in which the effects of cold work have disappeared, and the heat affected zone of the welded samples were examined under optical and scanning electron microscopes; additionally, mechanical tests and measures of Vickers microhardness were performed. Results showed dendritic morphology with solute micro- and macrosegregation in the fusion zone, which is favored by the constitutional supercooling when heat input increases. When heat input increased and welding speed increased or remained constant, greater segregation was obtained; whereas welding speed decrease produced a coarser microstructure. In the heat affected zone recrystallization, dissolution, and coarsening of precipitates occurred, which led to variations in hardness and strength.

Keywords: AA6105; cold work; GTAW; secondary phase; ultimate tensile strength; welding current; welding speed; weld bead hardness.

* M.Sc. Universidad Simón Bolívar (Caracas, Venezuela) midorta@usb.ve.
** M.Sc. Universidad Simón Bolívar (Caracas, Venezuela) mccapace@usb.ve.

Resumen

La soldadura con arco de tungsteno y gas (GTAW, sigla en inglés) es uno de los métodos más usados para soldar aluminio. En el presente trabajo se estudió la influencia de la corriente y la velocidad de soldadura en la microestructura y las propiedades mecánicas de la zona afectada por el calor de juntas de láminas de aluminio AA6105 con diferentes porcentajes de trabajo en frío soldadas por GTAW. También se evaluaron los cambios microestructurales en la zona de fusión, donde desaparece todo el historial del trabajo en frío. Las muestras fueron examinadas con microscopía óptica y electrónica de barrido; se realizaron ensayos de tracción y mediciones de dureza Vickers. En la zona de fusión se obtuvo una morfología dendrítica, con micro y macrosegregación de soluto, lo cual es favorecido por el superenfriamiento constitucional. Cuando aumentaron el calor aportado y la velocidad de soldadura, o esta última se mantuvo constante, fue mayor la segregación de soluto; mientras que con una disminución de la velocidad de soldadura la microestructura obtenida fue más gruesa. En la zona afectada por el calor se produjo recristalización, disolución o engrosamiento de precipitados, que originaron variaciones en la dureza y la resistencia máxima a tracción.

Palabras clave: AA6105; corriente de soldadura; GTAW; resistencia a la tensión; soldadura de aluminio; velocidad de soldadura.

Resumo

A soldadura com arco de tungstênio e gás (GTAW, sigla em inglês) é um dos métodos mais usados para soldar alumínio. Neste trabalho estudou-se a influência da corrente e a velocidade de soldadura na microestrutura e as propriedades mecânicas da zona afetada pelo calor de juntas de lâminas de alumínio AA6105 com diferentes porcentagens de trabalho em frio soldadas por GTAW. Também se avaliaram as alterações microestruturais na zona de fusão, onde desaparece todo o historial do trabalho em frio. As amostras foram examinadas com microscopia ótica e eletrônica de varredura; realizaram-se ensaios de tração e medições de dureza Vickers. Na zona de fusão obteve-se uma morfologia dendrítica, com micro e macrossegregação de soluto, o qual é favorecido pelo super-resfriamento constitucional. Quando aumentaram o calor aportado e a velocidade de soldadura, ou esta última se manteve constante, foi maior a segregação de soluto; enquanto que com uma diminuição da velocidade de soldadura a microestrutura obtida foi mais grossa. Na zona afetada pelo calor produziu-se recristalização, dissolução ou engrossamento de precipitados, que originaram variações na dureza e na resistência máxima a tração.

Palavras chave: AA6105; corrente de soldadura; GTAW; resistência à tensão; soldadura de alumínio; velocidade de soldadura.

I. Introduction

Aluminum is one of the most abundant metals in nature, and aluminum alloys are widely used in the industry due to their mechanical properties and corrosion resistance.

Aluminum is a difficult metal to weld due to the oxide layer that should be removed from its surface before welding. Gas Tungsten Arc Welding (GTAW) process is one of the methods used to weld aluminum because it is easy to apply, inexpensive, and produce high quality joints. This process is executed with the heat of an electric arc created between a non-consumable tungsten wire and the base metal in a shield of inert gas, usually argon, helium or a mixture of argon/helium, to protect the molten metal from the atmospheric contamination and prevent oxidation. If necessary, filler metal can be added externally to the arc in the form of a consumable wire [1].

Several investigations have analyzed the effect of welding parameters on the microstructure and mechanical properties of aluminum alloys. Singh *et al.* [2] studied the effect of welding current on hardness and microstructure of AA6082 aluminum alloy in GTAW, and found that hardness at low current was high and decreased as the current increased; moreover, hardness was low at nugget, and increased toward the base metal.

Gulshan and Ahsan [3] investigated GTAW welding of 1xxx series aluminum alloy to improve the structure – property relationship of weldment by controlling the heat input. Their results showed that at the highest current the eutectic mixture was coarser and larger in size and tended to form a continuous network. On the other hand, at low heat inputs the time was insufficient to let the eutectic mixture grow or form any continuous network. The change in microstructure with heat input was also supported by hardness, tensile, and impact strength [3].

Shah *et al.* [4] investigated the effect of a filler weld material on the mechanical properties of GTAW welded AA6061 alloy joints. They showed that samples welded with ER4043 have higher Vickers hardness and corrosion resistance compared to ER4047 samples [4].

Palani and Saju [5] studied the effect of GTAW welding parameters on welding of 65032 aluminum alloy. Based on their results, mathematical models have been developed to study the effect of process parameters on tensile strength and percent elongation. Furthermore, the authors conducted an optimization to find the best welding conditions to maximize tensile strength and percent elongation of the welded specimen [5].

Singh *et al.* [6] evaluated the effect of welding current, gas flow rate, and welding speed on the tensile strength of 5083 aluminum alloy. They showed that as welding speed increased tensile strength increased, first reaching the optimum value and then decreasing. Maximum tensile strength of weld joint was obtained at a current of 240 A, gas flow rate of 7 L/min, and welding speed of 98 mm/min [6].

Gautam [7] performed an optimization of process parameters for GTAW of AA1100 aluminum alloy using AC wave with argon as inert gas. The predicted optimum value of tensile strength of the weld joint determined by ANOVA and regression analysis was 91.35 MPa [7].

The effect of welding parameters on the microstructure and mechanical properties of aluminum alloys has been extensively investigated; nevertheless, the influence of these parameters on the heat affected zone of cold worked aluminum alloys has not been studied. In the construction of aluminum parts, the pieces are usually formed and cold worked to obtain the desired geometry, and then they are assembled through welding processes. To improve the performance of the parts manufactured in that way, studying the effect of welding on the microstructure and mechanical properties of the heat affected zone of cold worked aluminum alloys is important.

This research aims at studying the influence of welding parameters, such as welding current and welding speed, on the microstructure and mechanical properties of the heat affected zone of GTAW welded joints of AA6105 aluminum alloy with different levels of percent cold work. Additionally, it intends to investigate the effect of the mentioned parameters on the microstructure and hardness of the fusion zone, where the effects of cold work disappear due to solidification process, and constitutional supercooling influences the microstructural characteristics.

II. Experimental Method

A. Work material

The work material was the AA6105-T7 aluminum alloy, whose chemical composition is given in Table 1.

Table 1
Chemical composition of the work material (wt. %)

Si	Fe	Cu	Mn	Mg	Cr	Other	Al
0.748	0.200	0.020	0.002	0.580	0.001	-	Balance

B. Selection of work parameters

Welding current (I) and welding speed (S) were the welding parameters chosen according to the literature review [8]; additionally, the percent cold work (CW) was considered. Three levels (high, medium, and low) were selected for each parameter. The values of the process variables and their levels are listed in Table 2.

Plates of AA6105 alloy were rolled in a Stanat TA-315 rolling mill to obtain the cold work (CW) levels given in Table 2. 20, 30 and 50 % CW were obtained from 11.25, 7.5, and 7 mm thick plates, respectively. The rolling was performed at ambient temperature, with a reduction of thickness of 0.3175 mm per pass, and speed of 762 cm/min.

Table 2
Work parameters and their levels

Level	CW (%)	I (A)	S (mm/min)
Low	20	125	223
Medium	30	140	259
High	50	150	305

The orthogonal array L9 given in Table 3 was developed to establish the experimental conditions and obtain results in the "bigger the better" band. For each condition, the corresponding value of heat input (HI) is shown.

Table 3
Taguchi orthogonal array L9

Condition	CW (%)	I (A)	S (mm/min)	HI (KJ/mm)
1	20	125	223	0.673
2	20	140	259	0.649
3	20	150	305	0.590
4	30	125	259	0.579
5	30	140	305	0.551
6	30	150	223	0.807
7	50	125	305	0.492
8	50	140	223	0.753
9	50	150	259	0.695

C. Weld of the samples

From the plates rolled with 20, 30 and 50 % cold work, plates of 125 x 50.8 mm were cut. After rolling, the plates were machined to a uniform thick of 3.33 mm. The plates with a square joint design were butt joined with the GTAW process employing the Miller Syncrowave 250DX machine, with AC current, a constant voltage of 20 + 2 V, and argon as shielding gas. The filler material was an ER4043 wire with diameter of 2.38 mm; its chemical composition is presented in Table 4 [9].

Table 4
Chemical composition of ER4043 wire (wt. %)

Si	Fe	Cu	Mn	Cr	Ni	Zn	Ti	Mg	Al
4.5-6.0	0.8	0.30	0.05	-	-	0.10	0.20	0.05	Balance

Figure 1 shows a diagram of the welded plates, which were sectioned into two parts of 25 x 250 mm in order to obtain samples for tensile tests, microhardness measures, and microstructural analysis.

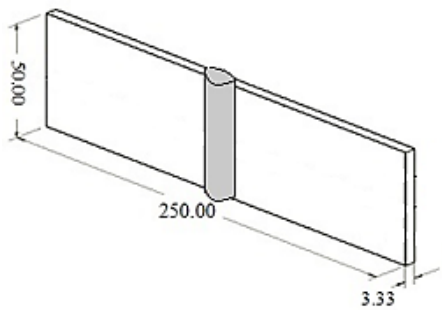

Fig. 1. Diagram of welded plates (dimensions in mm).

D. Microstructural analysis

The welded samples were prepared in their cross section according to ASTM E3 standard [10]. Specimens were cold mounted for easier handling, and etching was accomplished with 2% hydrofluoric acid (HF) for 3.5 minutes. Subsequently, the specimens were observed with the Olympus PMG3 optical microscope coupled with an Olympus DP12 camera and the JEOL JSM-6390 scanning electron microscope.

E. Tensile tests

Plain samples for tensile tests with the dimensions shown in Figure 2 were fabricated from the welded plates, according to ASTM B557 standard [11]. The tensile tests were performed on the MTS 312.31 universal testing machine, with speed of 5 mm/min.

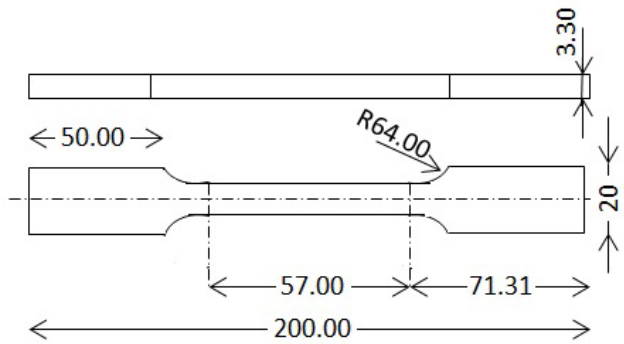

Fig. 2. Samples for tensile tests (dimensions in mm) [11].

F. Microhardness measure

The polished samples were used to measure Vickers microhardness. The samples were measured from the weld bead center to the heat affected zone, with an approximate separation of 0.3 mm between measures, using the Buehler Indentamet 1100 series hardness tester with a pyramidal diamond indenter and applying 100 gf by 30 s. Moreover, Vickers microhardness measures were taken in the as-received and the cold worked material.

III. Results

A. Microstructural analysis

Figure 3 shows the microstructural deformations resulted from rolling the plates, and the change the cold work produced on the shape and orientation of the grains.

The Vickers microhardness of rolled samples with 20, 30 and 50 % cold work were 92.31, 97.22 and 105.13, respectively, while in the as-received material was 83.90. The increase in hardness with cold work is related to the augment of dislocation density, and the changes in grain morphology produced by deformation process. It can be seen that in cold worked samples precipitates are more elongated and dispersed throughout the grains; this effect is more significant with increased percent cold work, which contributes to rise hardness.

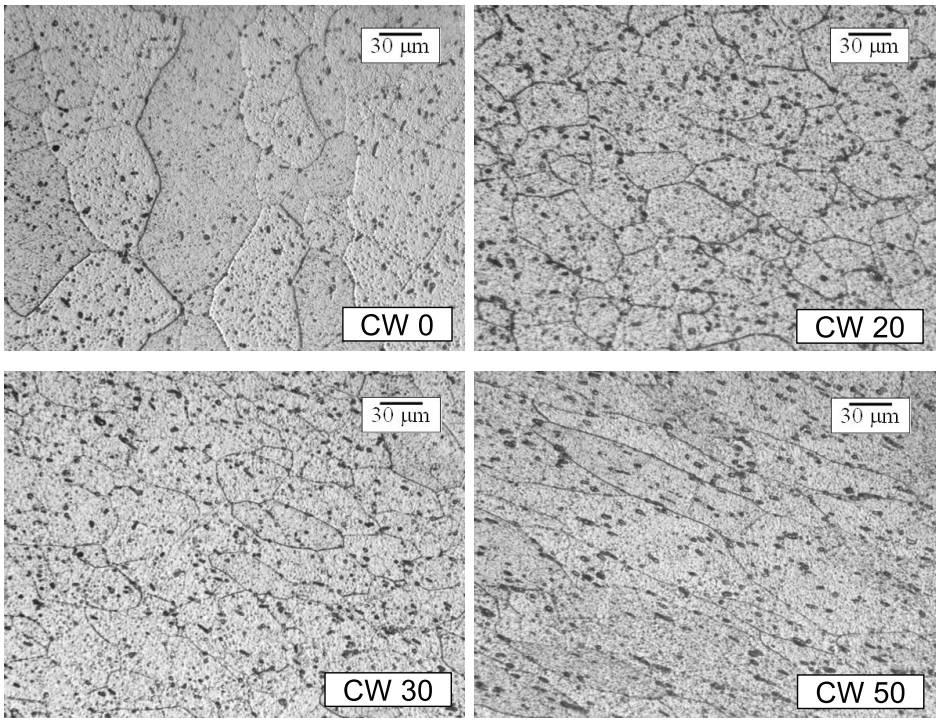

Fig. 3. Optical micrographs of AA6105 samples with different percent cold work, etched HF 2 %, magnification 100X.

Figure 4 shows the macrograph of the weld of sample 9 (CW 50 %, I 150 A, S 259 mm/min), indicating the base metal (BM) with a microstructure highly deformed, the heat affected zone (HAZ), in which a recrystallization process has taken place, and the fusion zone (FZ) with typical solidification process structures.

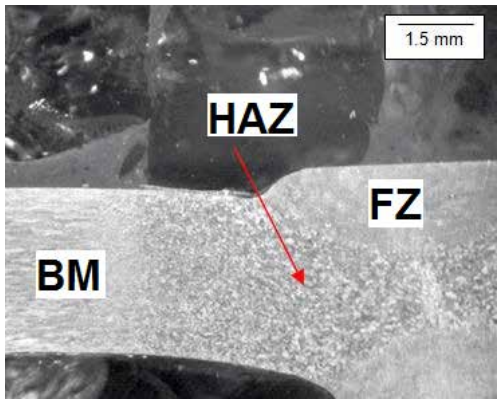

Fig. 4. Macrograph of sample 9 (CW 50 %, I 150 A, S 259 mm/min).

Figure 5 shows the difference in grain size in the heat affected zone of samples with 50 % cold work. In Figure 5a, which corresponds to sample 8 (I 140 A, S 223 mm/min), the average grain size, determined by procedures of ASTM E – 112 - 13 standard [12], is greater (80 µm) due to the low welding speed that generated higher heat input and slow cooling, improving the nucleation and growth of deformation free grains at the expense of the deformed grains [1]. In Figure 5b, which corresponds to sample 9 (I 150 A, S 259 mm/min), the average grain size is 30 µm due to the welding speed increase, which produced lower heat input and increased the cooling rate resulting in insufficient energy for grain growth. In both micrographs, it can be seen that near the fusion zone the grain size is bigger due to the higher temperatures that contribute with the nucleation and growth of recrystallized grains [13]. The dissolution of precipitates in the heat affected zone can also be noted.

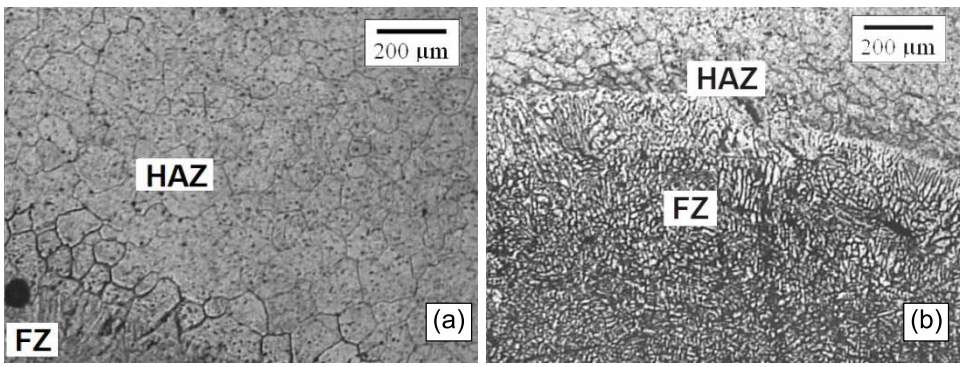

Fig. 5. Optical micrographs of HAZ and FZ: a) sample 8 (50 % CW, I 140 A, S 223 mm/min), b) sample 9 (50 % CW, I 150 A, S 259 mm/min), etched HF 2%, magnification 50X.

Figure 6 shows an optical micrograph of sample 6 (CW 30 %, I 150 A, S 223 mm/min). In the figure, the fusion zone and the heat affected zone, which have different microstructures due to the thermal processes during welding, can be distinguished. Additionally, the recrystallization and grain growth in the heat affected zone produced by temperature increase, and the columnar dendritic formation in the fusion zone, which is characteristic of aluminum alloy solidification can be seen. In the fusion zone, microsegregation produced by a solute rejection into the solid–liquid interface can be observed, as well as macrosegregation, which involves differences in solute composition in the zone that has been solidified.

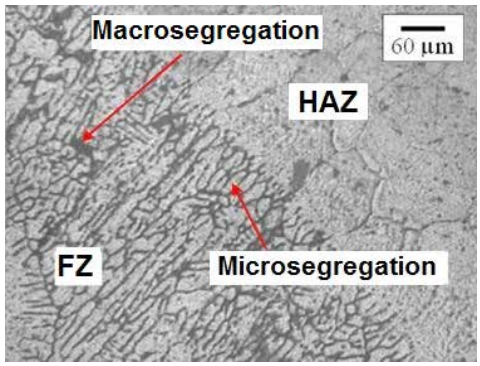

Fig. 6. Optical micrograph of HAZ and FZ of sample 6 (CW 30 %, I 150 A, S 223 mm/min), etched HF 2 %, magnification 100X.

The optical micrographs in Figure 7 show the fusion zone of samples welded with different combinations of current and welding speed. Columnar dendritic formation with solute macro- and microsegregation are observed in all the samples.

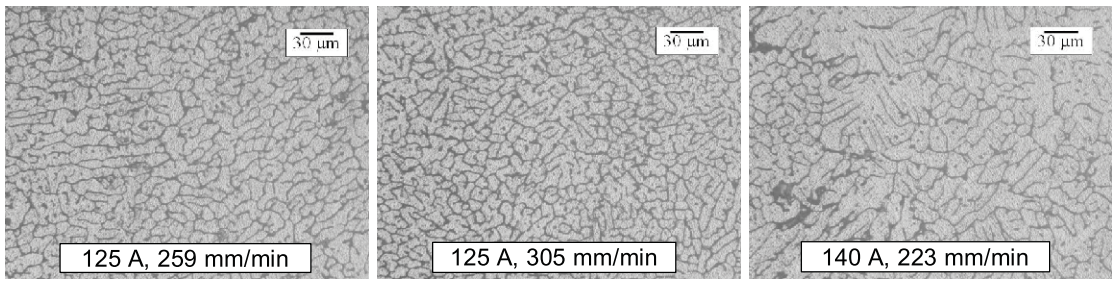

Fig. 7. Optical micrographs of FZ, etched HF 2 %, magnification 200X.

Figure 8 shows SEM micrographs of the fusion zone of samples 8 (CW 50 %, I 140 A, S 223 mm/min) and 7 (CW 50 %, I 125 A, S 305 mm/min). In both samples, the dendritic structure and solute enrichment in inter-dendritic spaces can be observed. In sample 7, the segregated solute is less abundant, coarse and continuous (Figure 8b) compared to sample 8 (Figure 8a). This is due to the increase of temperature gradient at the liquid–solid interface (G) that resulted from the reduction in heat input, leading to a decrease in constitutional supercooling [13].

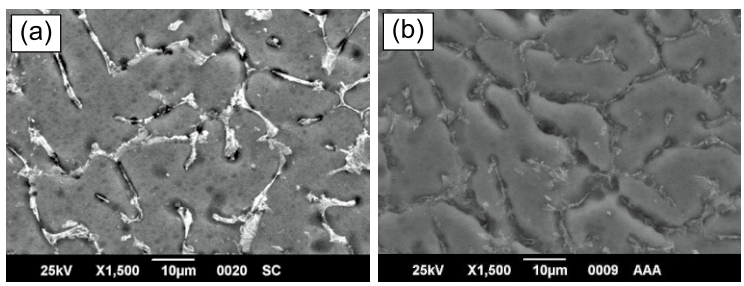

Fig. 8. SEM micrographs of FZ: a) sample 8 (50 % CW, I 140 A, S 223 mm/min), b) sample 7 (50 % CW, I 125 A, S 305 mm/min). Etched HF 2 %, magnification 1500X.

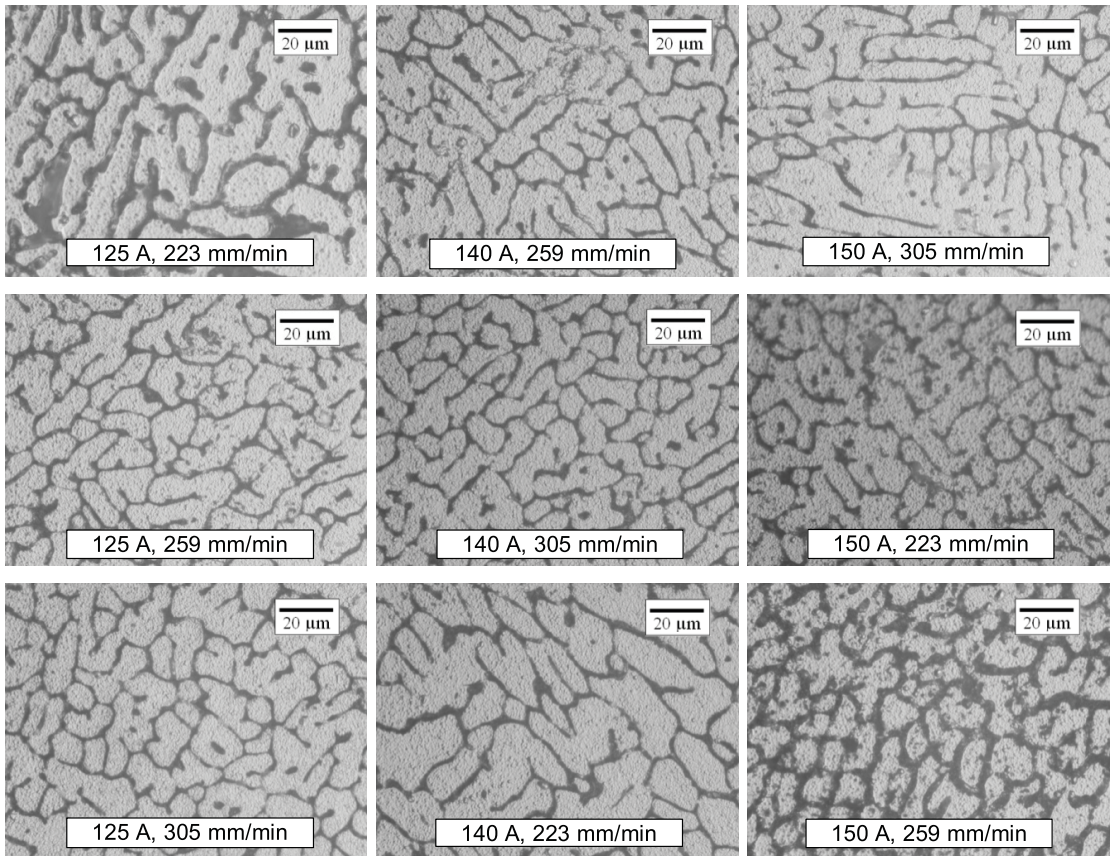

Fig. 9. Optical micrographs of FZ, etched HF 2 %, magnification 500X.

Figure 9 presents optical micrographs of the fusion zone in all samples welded with different parameter combination. It can be noted that the higher the welding speed is, under the same welding current, the finer the dendritic structure becomes. In this case, the growth rate (R) increased with the welding speed, and the temperature gradient at the liquid–solid interface raised due to the heat input decrease; hence a higher cooling rate (GxR) was obtained, which led to a finer structure. Regarding the G/R ratio, the trend is not clear since both, G and R, increased; therefore, it cannot be established which condition improved the G/R ratio to produce lower solute enrichment [13].

When G/R ratio is reduced, the constitutional supercooling in front of the advancing solid-liquid interface increases, and thus more solute is segregated to inter-dendritic regions. If the cooling rate GxR decreases, the structure becomes coarser. For current variation from 125 to 140 A with constant welding speed of 259 mm/min, the heat input augments led to a decrease in gradient temperature (G, Figure 9). When welding speed was constant, growth rate (R) did not vary, resulting in lower G/R and GxR [13].

B. Mechanical properties

Figure 10 shows the Vickers microhardness from the weld bead center to the heat affected zone in different samples. In all cases, hardness in the weld bead center was higher than in the heat affected zone. Sample 9 (CW 50 %, I 150 A, S 259 mm/min) had the highest hardness in the weld bead, followed by samples 3 (CW 20 %, I 150 A, S 305 mm/min) and 7 (CW 50 %, I 125 A, S 305 mm/min).

Hardness of sample 9 was greater than sample 7; sample 9 was welded with higher current and lower welding speed. As the heat input increased, the temperature gradient (G) decreased. Furthermore, as

the welding speed decreased, the solidification rate (R) also declined, which led to a cooling rate GxR reduction and a coarser structure. Since G and R were lower for sample 9, the variation of G/R ratio have an unclear tendency; however, as Figure 9 shows, sample 9 had more segregated solute, suggesting a lower G/R ratio [13]. The augment in solute led to a higher hardness of sample 9, although the structure was coarser.

Samples 7 and 3 were welded with the same welding speed resulting in the same growth rate; sample 7 was welded with lower current so the heat input was lower, leading to an increase in temperature gradient in liquid–solid interface. As a result, G/R and GxR raised, hence the amount of solute segregated to inter-dendritic regions was less and the structure was finer [13]. The decrease in hardness in the fusion zone of sample 7 suggests the reduction of segregated solute had a greater influence than the structure refinement.

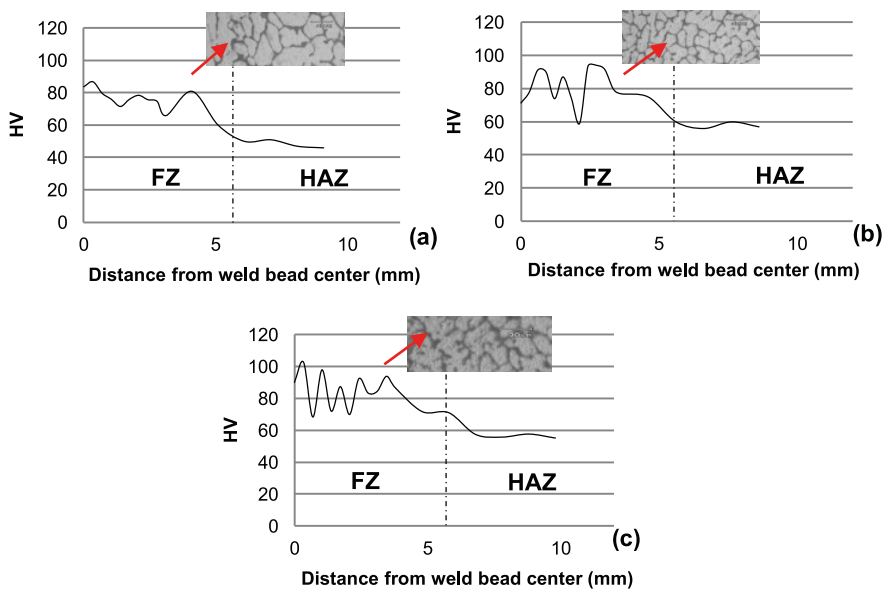

Fig. 10. Vickers microhardness from weld bead center to the HAZ, a) sample 3 (CW 20 %, I 150 A, S 305 mm/min, b) sample 7 (CW 50 %, I 125 A, S 305 mm/min, c) sample 9 (CW 50 %, I 150 A, S 259 mm/min.

Comparing the hardness in the heat affected zone of samples 7 and 9, which had the same initial percent cold work of 50 %, the hardness of sample 9, welded with increasing current and decreasing speed, was inferior. This is due to the higher heat input that reduces cooling rate, so the material spent more time at the recrystallization temperature, resulting in a larger growth of recrystallized grains than the one produced at lower hardness [2, 13]. In sample 3, which had smaller initial percent cold work, the hardness in the heat affected zone was lower. When cold work decreases, the growth of recrystallized grains is less, and hardness should be higher, suggesting that for sample 3 the hardness variation was governed by precipitate dissolution instead of recrystallization.

The temperature increase in the heat affected zone leads to dissolution of hardening phases present in base metal. However, near the fusion line, a partial recovery of hardness compared to base metal was obtained, possibly due to GP zones formation and precipitation of strengthening metastable phase β´´ during the storage time between welding and hardness measure [14-16]. In the utilisation of aluminium alloys for structural applications, one difficulty to be overcome is the reduction of mechanical properties of welded joints as compared to the parent material, consequent upon the weaker strength of the Weld Metal (WM).

Table 5 lists the mechanical properties of welded samples and alloy AA6105 (as-received and cold worked). Microhardness was measured in the weld

bead center. In all cases, the fracture occurred in the heat affected zone, whose hardness was lower than in the fusion zone (Figure 10) and the base metal. The ultimate tensile strength of welded samples was lower than the as-received material, due to dissolution of precipitates and recrystallization of heat affected zone.

Table 5

Mechanical properties of welded, as-received and cold worked samples

Sample	CW (%)	I (A)	S (mm/min)	Su (MPa)	HV
1	20	125	223	108.17	89.25
2	20	140	259	100.17	76.91
3	20	150	305	89.95	75.91
4	30	125	259	113.76	75.29
5	30	140	305	141.20	85.72
6	30	150	223	106.54	82.05
7	50	125	305	92.27	79.21
8	50	140	223	83.27	73.64
9	50	150	259	87.01	85.68
As-received	-	-	-	229.30	83.90
CW 20%	-	-	-	-	92.31
CW 30%	-	-	-	-	97.22
CW 50%	-	-	-	-	105.13

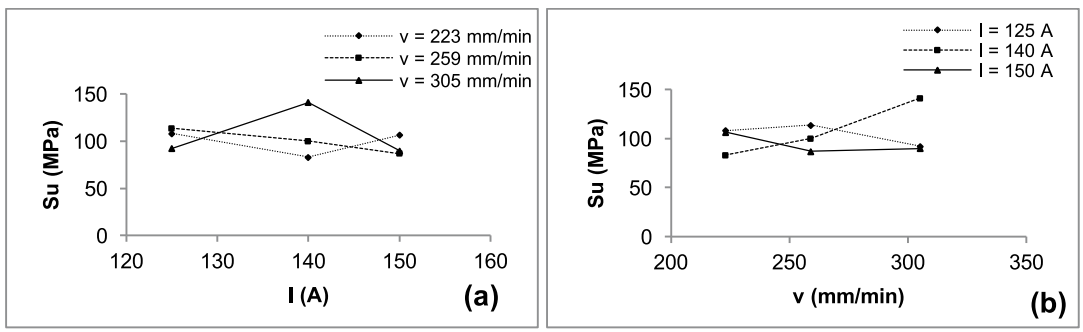

Fig. 11. Ultimate tensile strength variation with: a) welding current, b) welding speed.

Figure 11 shows the variation of ultimate tensile strength with welding current and speed. The higher the current, the higher the heat input, and hence recrystallized grain size augments due to the lower cooling rate, so strength decreases. Figure 11a illustrates this effect with welding speed of 259 mm/min; in this case, current and cold work augment occurred in the same direction, while with 223 and 305 mm/min strength raised with current increase from 140 to 150 A and from 125 to 140 A, respectively. In both cases, current increment was accompanied by a cold work reduction from 50 % to 30 %, so there was less stored energy available for recrystallized grain growth, reaching a lower grain size and a higher strength despite of the heat input increase.

At higher welding speed, heat input decreases and cooling rate is greater, leading to a lesser recrystallized grain size and a higher strength. Moreover, the temperature reached in the heat affected zone is lower, so there are undissolved precipitates, contributing to the strength increase. Strength increased with welding speed at current of 140 A, while it decreased at 125 and 150 A (Figure 11b). With 125 A, welding speed rise was accompanied by cold work augment; therefore, there was more stored energy that contributed to

recrystallized grain growth. If this effect prevails over the lesser recrystallized grain growth by heat input reduction, tensile strength reduces despite welding speed increase. With 150 A, welding speed variation from 223 to 259 mm/min led to a lower strength, probably due to this effect.

Current and welding speed variations can produce changes in precipitates in the heat affected zone. In AA6xxxx alloys, there are Al-Fe, Al-Mg and Fe-Si precipitates that can be dissolved or become coarser, depending on the temperature reached, which contributes to hardening or softening [17, 18].

Figure 12 shows the values of Taguchi signal-noise ratio in the "bigger the better" band of ultimate tensile strength for the three levels of percent cold work, welding current, and welding speed.

The values of the Signal-Noise Ratio in the "bigger the better" band, whose magnitude is higher, correspond to optimal welding conditions, so working with such parameters may result in higher values of ultimate tensile strength. Following this argument, it can be seen that maximum tensile strength was obtained with cold work of 30 % and low welding current. Regarding the welding speed, the signal-noise ratio obtained was similar with the three speed levels, and was higher for 305 mm/min.

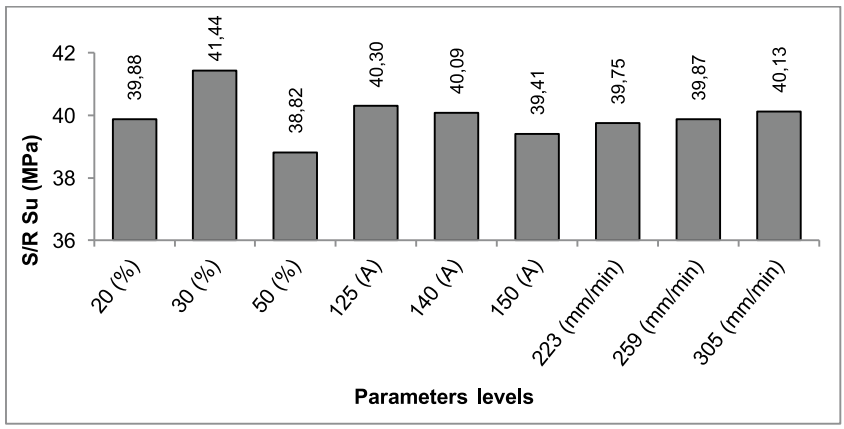

Fig. 12. Signal – noise ratio of ultimate tensile strength.

IV. Conclusions

This research obtained the following results for the microstructure and mechanical properties of GTAW AA6105 aluminum alloy welded joints:

- In the heat affected zone, bigger recrystallized grains were produced near the fusion zone, and smaller grains away from the weld bead.
- In the fusion zone, columnar dendritic structure with solute micro- and macrosegregation was observed.
- When welding speed increased at constant current, the dendritic structure of the fusion zone was finer.
- Current increase at constant welding speed produced greater solute segregation and coarser structure in the fusion zone.
- Hardness in the heat affected zone was lower than in the fusion zone and base metal, due to recrystallization and dissolution or coarsening of precipitates.
- At constant percent cold work, the lower the welding speed, the bigger the recrystallized grain size is in the heat affected zone.
- At constant percent cold work, if the current increased and the welding speed decreased, the hardness decreased; also, when percent cold work decreased, hardness increased.

- Current and percent cold work increased at a constant welding speed produced lower strength; in addition, if percent cold work decreased, strength augmented.

- Welding speed and percent cold work increase produced a decrease in strength, due to higher grain growth.

- When heat input increased, temperatures reached in the heat affected zone could be higher, leading to a decrease in strength due to precipitates dissolution.

References

[1] R. Messler, *Principles of Welding*. Singapore: John Wiley & Sons, 1999. DOI: http://dx.doi.org/10.1002/9783527617487.

[2] G. Singh, S. Kumar, and A. Singh, "Influence of Current on Microstructure and hardness of butt welding aluminium AA6082 using GTAW process," *Int. J. Res. Mech. Eng. Technol.*, vol. 3 (2), pp. 143-146, Oct. 2013.

[3] F. Gulshan and Q. Ahsan, "Effect of heat input on the structure and properties of aluminium weldment TIG welded with 4043 filler rod," *Chem. Mater. Eng.*, vol. 2 (2), pp. 25-32, 2014. DOI: http://dx.doi.org/10.13189/cme.2014.020201.

[4] L. H. Shah, N. Azhani, A. Razak, A. Juliawati, and M. Ishak, "Investigation on the mechanical properties of TIG welded AA6061 alloy weldments using different aluminium fillers," *Int. J. Eng. Technol.*, vol. 2 (2), pp. 116-120, Aug. 2013.

[5] P. K. Palani and M. Saju, "Modelling And optimization of process parameters for TIG welding of Aluminium-65032 using response surface methodology," *Int. J. Eng. Res. Appl.*, vol. 3 (2), pp. 230-236, 2013.

[6] L. Singh, R. Singh, N. K. Singh, D. Singh, and P. Singh, "An evaluation of TIG welding parametric influence on tensile strength of 5083 aluminium alloy," *Int. J. Mech. Aerospace, Ind. Mechatronics Eng.*, vol. 7 (11), pp. 1262-1265, 2013.

[7] V. Gautam, "Optimization of process parameters for Gas Tungsten Arc Welding of AA1100 Aluminium Alloy," *Int. J. Curr. Eng. Technol.*, vol. 4 (2), pp. 788-792, 2014.

[8] AWS, "Welding Handbook," *Fundamentals of Welding,* vol. 4. pp. 69.53-69, 1972.

[9] AWS, "A5.10 Specification for Bare Aluminum and Aluminum-Alloy Welding Electrodes and Rods." 2007.

[10] ASTM International, "ASTM E3-11, Standard guide for preparation of metallographic specimens," vol. 3 (1), 2011.

[11] ASTM International, "ASTM B557-14, Standard test methods for tension testing wrought and cast aluminum- and magnesium-alloy products," vol. 2 (2), 2014.

[12] ASTM International, "ASTM E112 - 13 Standard Test Methods for Determining Average Grain Size," vol. 3 (1), 2013.

[13] K. Sindo, *Welding Metallurgy*, 2da ed. USA: John Wiley & Sons, 2003.

[14] Y. Birol, "The effect of homogenization practice on the microstructure of AA6063 billets," *J. Mater. Process. Technol.*, vol. 148 (2), pp. 250-258, May. 2004. DOI: http://dx.doi.org/10.1016/j.jmatprotec.2004.01.056.

[15] S. Missori and A. Sili, "Mechanical behaviour of 6082-T6 aluminium alloy welds," *Metal. Sci. Technol.*, vol. 18 (1), pp. 12-18, 2000.

[16] H. Guo, J. Hu, and H. L. Tsai, "Formation of weld crater in GMAW of aluminum alloys," *Int. J. Heat Mass Transf.*, vol. 52 (23-24), pp. 5533–5546, Nov. 2009. DOI: http://dx.doi.org/10.1016/j.ijheatmasstransfer.2009.06.028.

[17] "ASM Handbook Volume 3: Alloy Phase Diagrams - ASM International." [Online]. Available: http://www.asminternational.org/online-catalog/phase-diagrams/-/journal_content/56/10192/06479G/PUBLICATION. [Accessed: 14-May-2016].

[18] M. Nicolas and A. Deschamps, "Characterisation and modelling of precipitate evolution in an Al–Zn–Mg alloy during non-isothermal heat treatments," *Acta Mater.*, vol. 51 (20), pp. 6077-6094, Dec. 2003. DOI: http://dx.doi.org/10.1016/S1359-6454(03)00429-4.